Approaching the Matched-Filter Bound Using Iterated-Decision Equalization with Frequency-Interleaved Encoding

Albert M. Chan and Gregory W. Wornell
Dept. EECS and Research Laboratory of Electronics
MIT, Cambridge, MA 02139

Abstract— **We propose a new low-complexity strategy for approaching the matched filter bound on most practical ISI channels. At the transmitter, a form of channel-independent precoding is introduced to perform frequency-interleaving, which appropriately conditions the channel. At the receiver, a very low-complexity iterated-decision equalizer [1] is used. As an illustration, we use the system to effectively attain the matched filter bound on the $1 + D$ channel without the use of error-control coding.**

I. Introduction

In this paper, we introduce a strategy for approaching the matched filter bound on practical intersymbol interference (ISI) channels with finite energy impulse responses. At the transmitter, frequency-interleaving is used as a precoding step, and we note that this precoding does *not* require any knowledge of the channel impulse response or the noise level. At the receiver, an iterated-decision equalizer [1] is used.

In Section II, we summarize the form of iterated-decision equalizer of interest, which exploits the receiver's knowledge of the channel impulse response [1]. In Section III, we develop "frequency-interleaved encoding," and describe how it can be used in conjunction with the iterated-decision equalizer. We analyze the performance and complexity of the proposed system in Sections III-A and III-B respectively. We emphasize that throughout this paper, the transmitter has no knowledge of the channel, which is usually the case for reasonably rapidly time-varying channels.

II. The Iterated-Decision Equalizer

In the discrete-time baseband model of the pulse amplitude modulation (PAM) communication system we consider, the transmitted data is a white stream of symbols $x[n]$, each with energy $\mathcal{E}_s$. The symbols $x[n]$ are corrupted by a convolution with the impulse response of the channel, $a[n]$, and by additive noise, $w[n]$, to produce the received symbols

$$r[n] = \sum_k a[k]x[n-k] + w[n]. \tag{1}$$

The impulse response $a[n]$ is normalized to have unit energy, and the noise $w[n]$ is a zero-mean, complex-valued, circularly symmetric, stationary, white Gaussian noise sequence with variance $\mathcal{N}_0$ that is independent of $x[n]$.

The iterated-decision equalizer processes the received data in a block-iterative fashion. Specifically, during each iteration or "pass," a linear filter is applied to a block of received data, and tentative decisions made in the previous iteration are then used to construct and subtract out an estimate of the ISI. The resulting ISI-reduced data is then passed on to a slicer, which makes a new set of tentative decisions. With each successive iteration, increasingly refined hard decisions are generated using this strategy.

The detailed structure of the iterated-decision equalizer is depicted in Fig. 1. The parameters of all systems and signals associated with the lth pass are denoted using the superscript l. On the lth pass of the equalizer where $l = 1, 2, 3, \ldots$, the received data $r[n]$ is first processed by a linear filter $b^l[n]$, producing the sequence

$$\tilde{r}^l[n] = \sum_k b^l[k]r[n-k]. \tag{2}$$

Next, an estimate $\hat{z}^l[n]$ of the ISI is constructed, where

$$\hat{z}^l[n] = \sum_k d^l[k]\hat{x}^{l-1}[n-k] \tag{3}$$

with $d^l[n]$ being a noncausal filter. (In subsequent analysis, we will show that $\hat{x}^0[n]$ is never required for the first iteration, so the sequence may remain undefined.) Since $\hat{z}^l[n]$ is intended to be some kind of ISI estimate, we restrict attention to the case in which $d^l[0] = 0$. The estimate $\hat{z}^l[n]$ is subtracted from $\tilde{r}^l[n]$ and the difference is scaled by $1/\mu^l$ to remove an estimation bias, i.e.,

$$\tilde{x}^l[n] = \frac{1}{\mu^l}(\tilde{r}^l[n] - \hat{z}^l[n]). \tag{4}$$

Finally, the slicer generates the hard decisions $\hat{x}^l[n]$ from $\tilde{x}^l[n]$ using a symbol-wise minimum-distance rule.

Since the equalizer uses a symbol-by-symbol decision device, a natural equalizer design strategy involves maximizing the signal-to-interference+noise ratio (SINR) at the slicer over all $B^l(\omega)$ and $D^l(\omega)$ at each iteration, where the SINR at the lth iteration is defined as

$$\gamma^l \triangleq \frac{\mathcal{E}_s}{E[|\tilde{x}^l[n] - x[n]|^2]}. \tag{5}$$

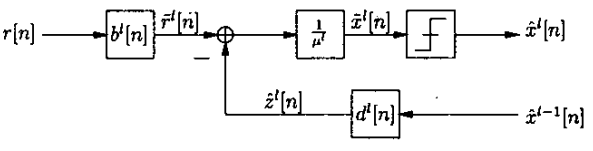

Fig. 1. Iterated-decision equalizer structure.

This work has been supported in part by ARL CTA No. DAAD19-01-2-0011, HP through the MIT/HP Alliance, and Texas Instruments through the Leadership Universities Program.

0-7803-7632-3/02/$17.00 ©2002 IEEE

Let $x[n]$ and $\hat{x}^{l-1}[n]$ be sequences of zero-mean uncorrelated symbols, each with energy $\mathcal{E}_s$; and let the normalized correlation between the two sequences be expressed in the form

$$\frac{E[x^*[n] \cdot \hat{x}^{l-1}[k]]}{\mathcal{E}_s} = \rho_x^{l-1}\delta[n-k]. \tag{6}$$

Then the optimal filters are

$$B^l(\omega) \propto \frac{A^*(\omega)}{\mathcal{N}_0 + \mathcal{E}_s(1-(\rho_x^{l-1})^2)|A(\omega)|^2} \tag{7}$$

$$D(\omega) = \rho_x^{l-1}\left(A(\omega)B^l(\omega) - \mu^l\right) \tag{8}$$

where

$$\mu^l = \frac{1}{2\pi}\int_{-\pi}^{\pi} A(\omega)B^l(\omega)d\omega. \tag{9}$$

The maximum SINR is thus

$$\gamma^l = \left(\frac{1}{\frac{1}{2\pi}\int_{-\pi}^{\pi}\frac{1}{1+\alpha^l(\omega)}d\omega} - 1\right)\cdot\frac{1}{1-(\rho_x^{l-1})^2} \tag{10}$$

where

$$\alpha^l(\omega) = \frac{\mathcal{E}_s(1-(\rho_x^{l-1})^2)|A(\omega)|^2}{\mathcal{N}_0}. \tag{11}$$

Furthermore, the slicer input $\tilde{x}^l[n]$ satisfies, for each n,

$$\tilde{x}^l[n] = x[n] + v^l[n] \tag{12}$$

where $v^l[n]$ is complex-valued, zero-mean, and uncorrelated with the input symbol stream $x[n]$, having variance

$$\text{var } v^l[n] = \frac{\mathcal{N}_0}{2\pi}\int_{-\pi}^{\pi}\left|\frac{B^l(\omega)}{\mu^l}\right|^2 d\omega + \frac{\mathcal{E}_s(1-(\rho_x^{l-1})^2)}{2\pi}\int_{-\pi}^{\pi}\left|\frac{A(\omega)B^l(\omega)}{\mu^l} - 1\right|^2 d\omega. \tag{13}$$

The optimal $D^l(\omega)$ is intuitively satisfying. The parameter ρ_x^{l-1} describes our confidence in the quality of the estimate $\hat{x}^{l-1}[n]$. If $\hat{x}^{l-1}[n]$ is a poor estimate of $x[n]$, then ρ_x^{l-1} will in turn be low, and consequently a smaller weighting is applied to the ISI estimate that is to be subtracted from $\tilde{r}^l[n]$. On the other hand, if $\hat{x}^{l-1}[n]$ is an excellent estimate of $x[n]$, then $\rho_x^{l-1} \approx 1$, and nearly all of the ISI is subtracted from $\tilde{r}^l[n]$. Note that the feedback branch is not used during the first pass because $\rho_x^0 = 0$, so the sequence $\hat{x}^0[n]$ does not need to be defined.

If the cascade of the ISI channel and l iterations of the equalizer is treated as an additive white Gaussian noise (AWGN) channel, then we have the following convenient iterative algorithm for determining the set of correlation coefficients ρ_x^l to be used at each iteration, and simultaneously predicting the associated sequence of symbol error probabilities:

1) Set $\rho_x^0 = 0$ and let $l = 1$.
2) Compute the SINR γ^l at the slicer input on the lth decoding pass from ρ_x^{l-1} via (10) and (11).
3) Approximate the symbol error probability $\Pr(\epsilon^l)$ at the slicer output from γ^l using the appropriate formula for the symbol error rate of a symbol-by-symbol threshold detector for AWGN channels [2]. For M-PSK,

$$\Pr(\epsilon^l) = 2\mathcal{Q}\left(\sin\left(\frac{\pi}{M}\right)\sqrt{2\gamma^l}\right), \tag{14}$$

where $\mathcal{Q}(v) = \frac{1}{\sqrt{2\pi}}\int_v^\infty e^{-t^2/2}dt$. For square M-QAM,

$$\Pr(\epsilon^l) = 1 - \left(1 - 2\left(1-\frac{1}{\sqrt{M}}\right)\mathcal{Q}\left(\sqrt{\frac{3\gamma^l}{M-1}}\right)\right)^2. \tag{15}$$

4) Compute the normalized correlation coefficient ρ_x^l between the symbols $x[n]$ and the decisions $\hat{x}^l[n]$ generated at the slicer via the approximation

$$\rho_x^l \approx 1 - 2\sin^2\left(\frac{\pi}{M}\right)\Pr(\epsilon^l) \tag{16}$$

for M-PSK or

$$\rho_x^l \approx 1 - \frac{3}{M-1}\Pr(\epsilon^l) \tag{17}$$

for square M-QAM.
5) Increment l and go to step 2.

III. The Iterated-Decision Equalizer with Frequency-Interleaved Encoding

The role of frequency-interleaving is to effectively transform any channel into a channel well-suited for use with the iterated-decision equalizer described in Section II.

Figure 2 depicts the cascade of the transmitter, ISI channel, and the receiver front end when frequency-interleaved encoding is used with the iterated-decision equalizer. At the transmitter, a sequence of N data symbols $x[n]$ is interleaved in the frequency domain, so that the time sequence $x_p[n]$ corresponding to the N-point discrete Fourier transform (DFT) $X_p[k]$ is obtained, where $X_p[k] \triangleq X[p(k)]$, $p(\cdot)$ is a permutation of the set $\mathcal{S} = \{0,1,2,\ldots,N-1\}$, and $X[k]$ is the DFT of $x[n]$. Appended to the time sequence is a cyclic prefix of length $L-1$, where L is the length of the channel impulse response and whose purpose will be explained shortly. The resulting signal $x_p[n]$ is transmitted over the ISI channel. The symbols $x_p[n]$ are corrupted by a convolution with the impulse response of the channel, $a[n]$, and by additive noise, $w[n]$, to produce the received symbols

$$r_p[n] = \sum_k a[k]x_p[n-k] + w[n]. \tag{18}$$

The impulse response $a[n]$ is normalized to have unit energy, and the noise $w[n]$ is a zero-mean, complex-valued, circularly symmetric, stationary, white Gaussian noise sequence with variance $\mathcal{N}_0$ that is independent of $x[n]$. At the receiver front end, the cyclic prefix is removed from the sequence $r_p[n]$, and

the remaining sequence is deinterleaved in the frequency domain, so that the N-point DFT $R[k]$ is obtained. The relationship between $R[k]$ and $X[k]$ is then

$$R[k] = A_{p^{-1}}[k]X[k] + W_{p^{-1}}[k], \tag{19}$$

where $A_{p^{-1}}[k] \triangleq A[p^{-1}(k)]$ and $W_{p^{-1}}[k] \triangleq W[p^{-1}(k)]$, $p^{-1}(\cdot)$ is the inverse permutation of $p(\cdot)$, and $A[k]$ and $W[k]$ are the DFTs of $a[n]$ and $w[n]$ respectively. Note that the use of a cyclic prefix causes $X[k]$ to be pointwise multiplied by $A_{p^{-1}}[k]$.

Though frequency-interleaved encoding has similarities with OFDM systems that do not know the channel at the transmitter, it is important to emphasize that the motivation and performance of the two are different. An uncoded OFDM system is designed to circumvent the need for equalization, but does not achieve the matched filter bound unless the attenuation in all subbands is equal (i.e., the channel is flat). Frequency-interleaved encoding, on the other hand, is related to a power- and bandwidth-efficient signal space diversity technique that makes transmitted signals insensitive to fading channels [3]. The DFT matrix operation at the transmitter in Fig. 2 is equivalent to the rotation matrix in [3], thereby creating a diversity order of up to N. The remaining blocks in Fig. 2 implement the pointwise multiplication of $X[k]$ with an interleaved version of $A[k]$. Interleaving destroys the correlation in $A[k]$, similar in purpose to the interleaving proposed in [3] to destroy correlation among the channel fading coefficents. As we will see later in this section, frequency-interleaved encoding can convert a channel for which maximum-likelihood sequence detection (MLSD) cannot achieve the matched filter bound into a channel for which the bound can be asymptotically approached. However, MLSD for a channel with N parameters is an intractable problem for large N.

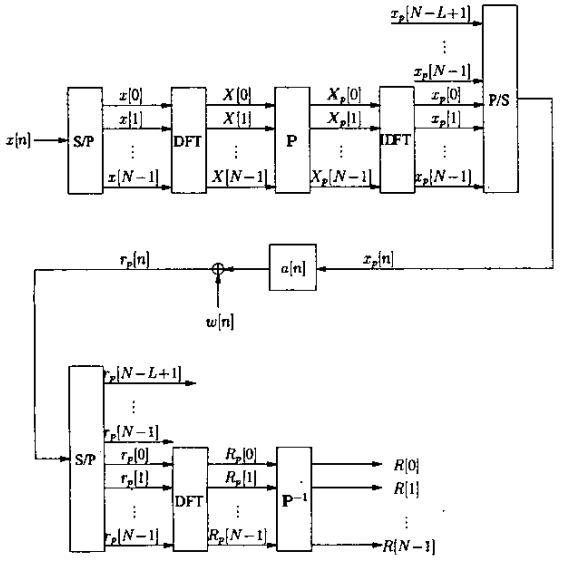

Fig. 2. The cascade of the transmitter, ISI channel, and receiver front end when frequency-interleaved encoding is used with the iterated-decision equalizer.

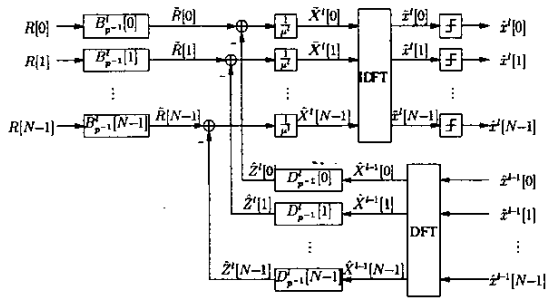

Fig. 3. The structure of the iterated-decision equalizer when frequency-interleaved encoding is used.

The equalizer described in Section II is a low-complexity technique that can be used after the receiver front end to approximate MLSD, with several modifications. First, the channel to be equalized is now $a_{p^{-1}}[n]$ rather than $a[n]$. Second, all the filtering is done in the DFT domain as illustrated in Fig. 3. Third, the integrals of Fourier transforms have been replaced by sums of the frequency samples of the corresponding DFTs. Thus, the optimal filters are

$$B^l_{p^{-1}}[k] \propto \frac{A^*_{p^{-1}}[k]}{\mathcal{N}_0 + \mathcal{E}_s(1-(\rho_x^{l-1})^2)|A_{p^{-1}}[k]|^2} \tag{20}$$

$$D^l_{p^{-1}}[k] = \rho_x^{l-1}\left(A_{p^{-1}}[k]B^l_{p^{-1}}[k] - \mu^l\right) \tag{21}$$

where

$$\mu^l = \frac{1}{N}\sum_{i=0}^{N-1} A[i]B^l[i], \tag{22}$$

and the maximum SINR is

$$\gamma^l = \left(\frac{1}{\frac{1}{N}\sum_{k=0}^{N-1}\frac{1}{1+\alpha^l[k]}} - 1\right)\cdot\frac{1}{1-(\rho_x^{l-1})^2} \tag{23}$$

where

$$\alpha^l[k] = \frac{\mathcal{E}_s(1-(\rho_x^{l-1})^2)|A[k]|^2}{\mathcal{N}_0}. \tag{24}$$

The slicer input $\tilde{x}^l[n]$ satisfies, for each n,

$$\tilde{x}^l[n] = x[n] + v^l[n] \tag{25}$$

where $v^l[n]$ is complex-valued, zero-mean, and uncorrelated with the input symbol stream $x[n]$, having variance

$$\text{var } v^l[n] = \frac{\mathcal{N}_0}{N}\sum_{k=0}^{N-1}\left|\frac{B^l[k]}{\mu^l}\right|^2 + \frac{\mathcal{E}_s(1-(\rho_x^{l-1})^2)}{N}\sum_{k=0}^{N-1}\left|\frac{A[k]B^l[k]}{\mu^l} - 1\right|^2. \tag{26}$$

Furthermore, the iterative algorithm for determining the sequence of ρ_x^l remains the same as in Section II, except that γ^l is now computed in Step 2 from ρ_x^{l-1} via (23) and (24).

For the remainder of this paper, we consider the special case in which $p(\cdot)$ is a random permutation of the set $\mathcal{S} = \{0, 1, 2, \cdots, N-1\}$, with all permutations being equally likely. In this case, the frequency-interleaving creates an effective channel that has some special properties. In particular, it can be shown that the coefficients of the resulting effective channel $a_{p^{-1}}[n]$ are uncorrelated. Given that the effective channel can be expressed as

$$a_{p^{-1}}[n] = \frac{1}{N}\sum_{k=0}^{N-1} A_{p^{-1}}[k]e^{j\frac{2\pi k}{N}n} = \frac{1}{N}\sum_{k=0}^{N-1} A[k]e^{j\frac{2\pi p(k)}{N}n} \tag{27}$$

for $0 \le n \le N-1$, the second-order statistics are given by $E[a_{p^{-1}}[n]] = a[0]\delta[n]$ and

$$E[a_{p^{-1}}[n]a^*_{p^{-1}}[m]] = \begin{cases} |a[0]|^2 & n = m = 0 \\ \frac{1}{N-1}\sum_{i=1}^{N-1}|a[i]|^2 & n = m \neq 0 \\ 0 & \text{otherwise} \end{cases} \tag{28}$$

where the expectations are over all permutations.

In light of the fact that the coefficients of the effective channel $a_{p^{-1}}[n]$ are uncorrelated, it is reasonable to expect that the effective noise process $v^l[n]$ at the slicer input becomes white in the limit as $N \to \infty$. This is indeed the case, as described by the following theorem whose proof is in [4] and is omitted due to space constraints.

Theorem 1: Let p be a random permutation of the set $\mathcal{S} = \{0, 1, 2, \ldots, N-1\}$, with all permutations being equally likely. Then, as $N \to \infty$, we have that the slicer input $\tilde{x}^l[n]$ in (25) satisfies, for each n, [1]

$$\tilde{x}^l[n] \xrightarrow{\text{m.s.}} x[n] + v^l[n] \tag{29}$$

where $v^l[n]$ is not only a complex-valued, zero-mean sequence uncorrelated with $x[n]$ having variance (26), but also a sequence that is marginally Gaussian and white.

Thus, treating the cascade of the frequency-interleaved channel with the equalizer as an AWGN channel in Step 3 of the iterative algorithm for determining ρ_x^l is reasonably well justified. Note also that $(L-1)/N \to 0$ as $N \to \infty$, so the overhead for the cyclic prefix becomes negligible.

Essentially, the system described in this section transforms an arbitrary ISI channel into a "good" channel with very high probability, where "good" means that the matched filter bound can be asymptotically achieved at high signal-to-noise ratio (SNR) using the equalizer described in Section II.

A. Performance

For illustration purposes, our simulations and plots in this section are based on the $1+D$ channel (i.e., $a[n] = \delta[n]/\sqrt{2} + \delta[n-1]/\sqrt{2}$) with $N = 256$ and $L = 2$, unless otherwise stated.

The analysis of the iterative nature of the equalizer is analogous to the analysis presented in [1]. From Steps 2 and 3 of the algorithm to compute ρ_x^l, we see that $\Pr(\epsilon^l)$ can be expressed as $\Pr(\epsilon^l) = \mathcal{G}(\zeta, \rho_x^{l-1})$ where $1/\zeta$ is defined as the received SNR, $\mathcal{E}_s/\mathcal{N}_0$. In Fig. 4, the successively lower solid curves plot $\mathcal{G}(\zeta, \rho_x)$ as a function of $1/(1-\rho_x)$ for various values of $1/\zeta$. Meanwhile, from Step 4 of the algorithm, $\Pr(\epsilon^l)$ can be expressed as $\Pr(\epsilon^l) = \mathcal{H}(\rho_x^l)$, which corresponds to the dashed line in Fig. 4. At a given SNR $1/\zeta$, the sequence of error probabilities $\Pr(\epsilon^l)$ and correlation coefficients ρ_x^l can be obtained by iterating horizontally and vertically between the appropriate solid curve and the dashed line. The error rate performance for a given $1/\zeta$ eventually converges to a steady-state value of $\Pr(\epsilon^\infty)$, corresponding to the intersection of the dashed line and the appropriate solid curve in Fig. 4. It is significant that few passes are required to approximately achieve steady state, since the amount of computation is directly proportional to the number of passes required.

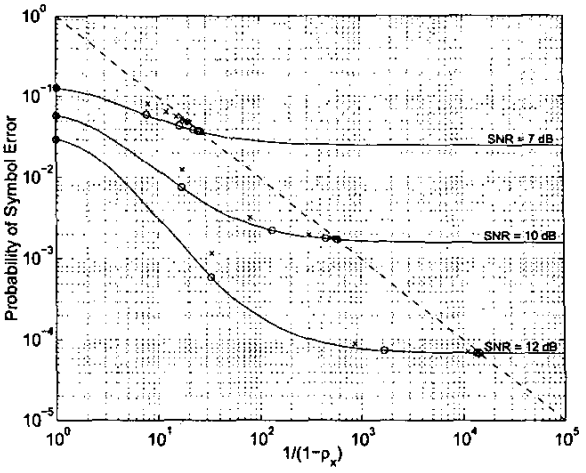

Fig. 4. Iterated-decision equalizer performance with frequency-interleaved encoding. The successively lower solid curves plot QPSK symbol error rate as a function of ρ_x for the $1+D$ channel at SNR's of 7,10, and 12 dB respectively. Along each curve, o's identify the theoretically predicted decreasing error rates achieved with $l = 1, 2, \ldots$ decoding passes, and the intersections with the dashed line are the steady-state values ($l \to \infty$). The associated experimentally obtained values are depicted using ×'s.

We now discuss the high-SNR ($\zeta \to 0$) limit of the SINR expression in (23) for fixed ρ_x. For a particular channel $A[k]$, let β be the ratio of the total number of DFT points, N, to the number of nonzero DFT points. As $\zeta \to 0$ with ρ_x fixed, it can be shown [4] that

$$\gamma \to \frac{1}{\beta - 1} \cdot \frac{1}{1 - (\rho_x)^2}. \tag{30}$$

Since this limit is approached from below, it is a convenient upper bound on γ for any ζ.

The limit of (23) as $\rho_x \to 1$ for fixed ζ has also been shown [4] to be

$$\gamma \to \frac{1}{\zeta}. \tag{31}$$

Thus (30) and (31) are two upper bounds on γ, correspond-

[1] We use the notation $\xrightarrow{\text{m.s.}}$ to denote convergence in the mean-square sense.

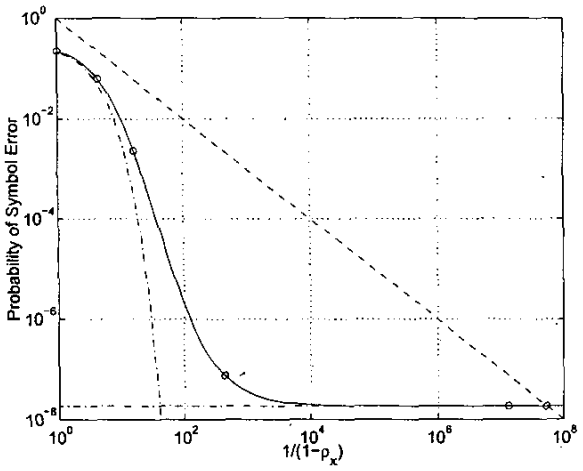

Fig. 5. High SNR performance limits of the iterated-decision equalizer with frequency-interleaved encoding. The solid curve plots the QPSK symbol error rate as a function of ρ_x for a bandpass channel with $\beta = 1.641$ at an SNR per bit of 12 dB, and o's identify the theoretically predicted decreasing error rates. The dash-dot curves indicate the high-SNR limits of performance.

ing to lower bounds on $\Pr(\epsilon)$. These bounds are illustrated in Fig. 5 for an ideal bandpass channel with $\beta = 1.641$, where the solid curve corresponds to (23), the dash-dot horizontal line corresponds to (31), and the dash-dot curve corresponds to (30).

We now examine the conditions under which the iterated-decision equalizer with frequency-interleaved encoding can achieve the matched filter bound. First, from Fig. 5, we observe that a necessary condition for the matched filter bound to be achieved is that the dash-dot curve corresponding to (30) lie completely below the dashed curve. This is the case for virtually all practical fullband channels, where $\beta \approx 1$. Second, the convergence in (31) must occur for small enough values of $1/(1-\rho_x)$ so that $\gamma^{\infty} \approx 1/\zeta$; i.e., convergence of the solid curve to the horizontal dash-dot curve in Fig. 5 must occur to the left of the dashed curve. This is indeed the case at high SNR, as shown in [4].

In Fig. 6, we present the bit-error rate as a function of SNR for the iterated-decision equalizer with frequency-interleaved encoding. The iterated-decision equalizer with frequency-interleaved encoding clearly outperforms various other equalizers, including MLSD and the iterated-decision equalizer without encoding, and indeed approaches the matched filter bound at high SNR.

One might wonder whether frequency-interleaved encoding can be used with various other equalizers to produce a similar gain in performance. In fact, if such encoding is used in conjunction with a linear equalizer (LE) or decision-feedback equalizer (DFE), there is no change in performance. The reason is that the channel affects the mean square slicer error of both kinds of equalizers via a frequency average [5], which remains constant whether the channel is $A[k]$ or $A_{p^{-1}}[k]$.

B. Complexity

Without frequency-interleaving, systems with iterated-decision equalization have a complexity that is essentially linear in block length N for a given channel and SNR. When frequency interleaving is incorporated, the complexity is proportional to $N \log N$. However, the complexity does not depend directly on the constellation size. By contrast, the Viterbi algorithm which implements MLSD has complexity NM^L, where M is the signal constellation size and L is the length of the channel.

The actual savings can be dramatic in practice on typical channels. For example, when $N = 256$, $M = 4$, and $L = 5$, and we perform 10 iterations of the iterated-decision equalizer (which is typically more iterations than needed), the iterated-decision equalizer with frequency-interleaved encoding is roughly an order of magnitude less complex than the Viterbi algorithm with the same parameters. The difference is even more dramatic with larger signal constellations. When M is increased to 64, the complexity of the iterated-decision equalizer with frequency-interleaved encoding remains unchanged, but the Viterbi algorithm becomes an additional 6 orders of magnitude more complex.

References

[1] A. M. Chan and G. W. Wornell, "A class of block-iterative equalizers for intersymbol interference channels: Fixed channel results," *IEEE Trans. Commun.*, vol. 49, Nov. 2001, pp. 1966–1976.

[2] J. G. Proakis, *Digital Communications*, 3rd ed. New York: McGraw-Hill, 1995.

[3] J. Boutros and E. Viterbo, "Signal space diversity: A Power- and bandwidth-efficient diversity technique for the Rayleigh fading channel," *IEEE Trans. Inform. Theory*, vol. 44, July 1998, pp. 1453–1467.

[4] A. M. Chan and G. W. Wornell, "Approaching perfect interference cancellation using iterated-decision receivers with mode-interleaved encoding," preprint.

[5] E. A. Lee and D. G. Messerschmitt, *Digital Communication*, 2nd ed. Boston, MA: Kluwer, 1994.

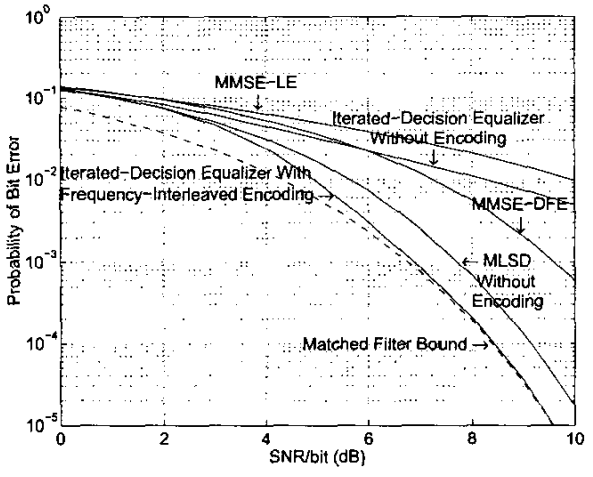

Fig. 6. Experimentally observed performance for various equalizers. The solid curves depict QPSK bit-error rates for the $1 + D$ channel as a function of SNR per bit.